Self-Assembled Squalenoylated Penicillin Bioconjugates: An Original Approach for the Treatment of Intracellular Infections

Nicolas Sémiramoth,[†,#] Chiara Di Meo,[†,#] Fatima Zouhiri,[†] Fatouma Saïd-Hassane,[†] Sabrina Valetti,[†] Roseline Gorges,[§] Valérie Nicolas,[⊥] Jacques H. Poupaert,[∥] Sylvie Chollet-Martin,[§] Didier Desmaële,[‡] Ruxandra Gref,[†] and Patrick Couvreur[†,*]

[†]Faculty of Pharmacy, UMR CNRS 8612, University of Paris-Sud XI, 5 Rue Jean-Baptiste Clément, 92296 Châtenay-Malabry Cedex, France, [‡]Faculty of Pharmacy, UMR CNRS 8076 Biocis, University of Paris-Sud XI, 5 Rue Jean-Baptiste Clément, 92296 Châtenay-Malabry Cedex, France, [§]Faculty of Pharmacy, INSERM UMRS 996, University of Paris-Sud XI, 5 Rue Jean-Baptiste Clément, 92296 Châtenay-Malabry Cedex, France, [⊥]Faculty of Pharmacy, INSERM IFR 141, University of Paris-Sud XI, 5 Rue Jean-Baptiste Clément, 92296 Châtenay-Malabry Cedex, France, and [∥]Louvain Drug Research Institute, UCLouvain, Avenue E. Mounier 73, B-1200 Brussels, Belgium. [#]Equally contributing first authors.

ABSTRACT We describe here new nanoparticles based on the bioconjugation of penicillin G to squalene in order to overcome severe intracellular infections by pathogen bacteria whose mechanism of resistance arises from the poor intracellular diffusion of several antibiotics. Two different squalene—penicillin G conjugates were synthesized (pH-sensitive and pH-insensitive), and their self-assembly as nanoparticles was investigated through morphology and stability studies. These nanoparticles had a size of 140 ± 10 nm (polydispersity index of 0.1) and a negative charge, and they did not display any supramolecular organization. Furthermore, they were found stable in water and in different culture medium. The cellular uptake and localization of these fluorescently labeled nanoparticles were explored on the macrophage cell line J774 by flow cytometry and confocal microscopy analysis. The squalenoylated nanoparticles were found to be cell internalized through clathrin-dependent and -independent endocytic pathways. Moreover, they induced an improved intracellular antibacterial activity on the facultative intracellular pathogen *S. aureus*, compared with free penicillin G, despite the absence of co-localization between the bacteria and the nanoparticles in the cells. This study suggests that the bioconjugation of an antibiotic to a squalene template could be a valuable approach for overcoming the antibiotic resistance due to intracellular bacterial infections.

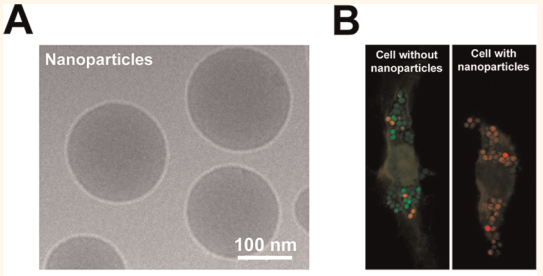

Nanoparticles made of Penicillin G-Squalene bioconjugates (A) efficiently kill intracellular bacteria (live bacteria in green, dead bacteria in red) (B)

KEYWORDS: nanoparticle · squalene · antibiotic · penicillin G · intracellular infections

Major problems associated with severe bacterial infections are related to the existence of intracellular pathogens and to the acquisition of antibiotic resistance by these bacteria. In fact, several obligatory and facultative intracellular bacteria are able to survive and multiply within phagocytic cells, which become reservoirs of pathogenic bacteria, giving rise to chronic infections.[1]

Therefore, there is a tremendous interest in improving antibiotics' entry within cells, in order to treat these intracellular infectious diseases.[2] In particular, many efforts have been made in the last decades in order to find a useful carrier for the intracellular delivery of beta-lactam antibiotics. These antibiotics are, indeed, widely used to treat infections caused by various pathogens, but they have low intracellular uptake in phagocytic cells because of their weak acidic character (*i.e.*, they are ionized at neutral physiological pH), and they do not diffuse spontaneously through cell membranes. Nanoparticulate carriers have been considered to transport antibiotics into phagocytic cells,[3] and in particular, antibiotic-loaded liposomes have been extensively studied.[4] Also, Couvreur *et al.* synthesized polyalkylcyanoacrylate nanoparticles (NPs) loaded with ampicillin for the treatment of *Listeria* and *Salmonella* spp. intracellular infections.[5,6] These nanoparticles allowed the antibacterial activity of the antibiotic against intracellular infections to increase by 120 times *in vivo*, due to the improved cellular uptake and to the accumulation of the antibiotic-loaded nanoparticles within the reticuloendothelial system (RES). However, the drug loading was poor, which necessitated the administration of high amounts of polymer to reach sufficient intracellular concentrations of the antibiotic. This has resulted in some toxicity and side effects, due to intracellular overloading of the cyanoacrylic polymer.

In order to overcome this important toxicological limitation, we have synthesized

* Address correspondence to patrick.couvreur@u-psud.fr.

Received for review December 16, 2011 and accepted April 6, 2012.

Published online April 06, 2012
10.1021/nn204928v

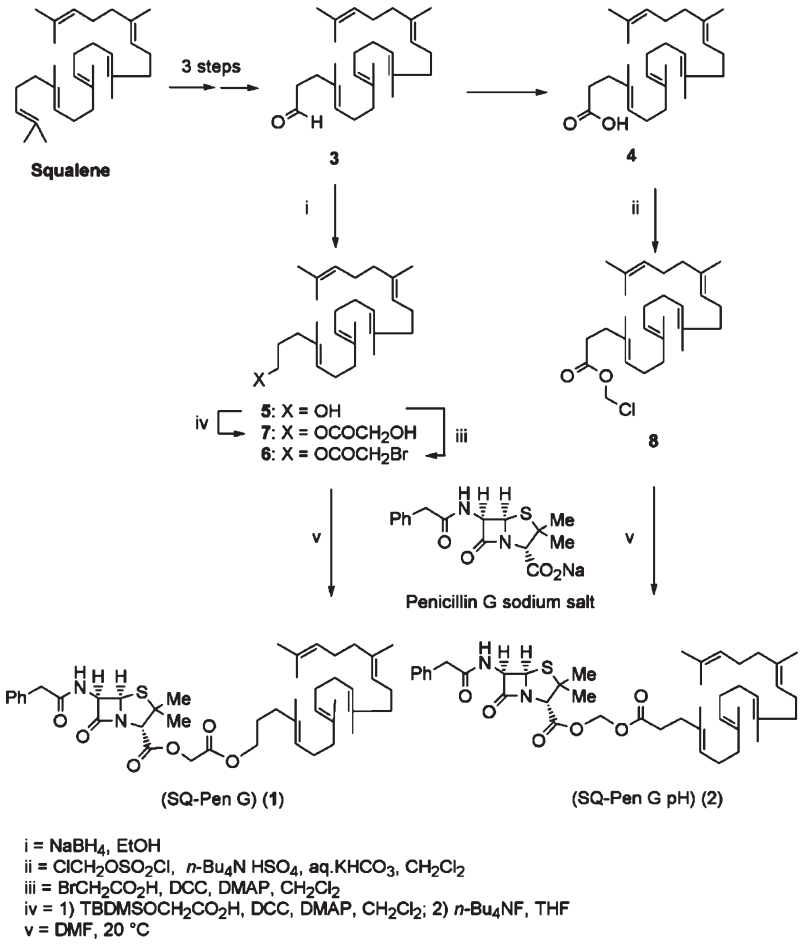

Scheme 1. Synthetic scheme of penicillin G squalenyl conjugates 1 and 2.

here new amphiphilic derivatives based on benzylpenicillin (PNG) linked to squalene (Sq) through pH-sensitive or pH-insensitive chemical bonds. The two bioconjugates differed in the nature of the linker between the hydrophobic chain and the penicillin G polar head. In the first compound, the ester bond was less labile than in the second, which was hydrolyzable in a pH-dependent manner. Remarkably, these new bioconjugates were able to spontaneously self-assemble in aqueous media as NPs, yielding impressive antibiotic loading (44 wt %). Noteworthy, the unique property of the natural lipid squalene to allow the formation of nanoparticles after conjugation was already observed with gemcitabine, an anticancer compound.[7]

This paper also investigates the morphology of the obtained NPs, their cell uptake, and their improved antibacterial activity against intracellular infections by *Staphylococcus* strain.

RESULTS AND DISCUSSION

Synthesis of Squalenyl–Penicillin G Conjugates. The squalenyl conjugate SqPNG (**1**) and the pH-sensitive one, SqPNG-pH (**2**), were synthesized by alkylation of the carboxylate function of penicillin G (**4**) with bromoacetate **6** and chloromethyl ester **8**, respectively, according to Scheme 1. Thus, 1,1′,2-trisnorsqualene alcohol (**5**) was first prepared in four steps from squalene *via* the trisnorsqualene aldehyde according to the Prestwich procedure.[8] Condensation of **5** with bromoacetic acid using N,N′-dicyclohexylcarbodiimide (DCC) as coupling agent led to the corresponding bromoester **6** in 70% yield. Coupling of penicillin G (PNG) sodium salt with bromoacetate **6** took place smoothly in DMSO to provide conjugate **1** in 34% yield. However, simple esters of penicillin are usually not prodrugs of β-lactam antibiotics since the ester bond is not easily cleaved. In contrast, acyloxymethyl esters such as pivampicillin are known to be extremely sensitive to chemical and enzymatic hydrolysis.[9,10] Therefore, we prepared the new conjugate **2** designed to release penicillin G within acidic subcellular organelles such as lysosomes. The chloromethyl ester of 1,1′,2-trisnorsqualenic acid (**8**) was first prepared upon treatment of trisnorsqualenic acid (**4**)[8] with chloromethanesulfonyl chloride.[11] Subsequent alkylation of the sodium salt of penicillin G afforded conjugate **2** in 49% yield. Both squalenoyl conjugates **1** and **2** were found quite stable, surviving chromatographic purification over silica gel and were fully characterized by spectroscopic methods. Since enzymatic hydrolysis of **1** is likely to release hydroxyacetic acid

squalenyl ester **7**, an authentic sample of this material was synthesized by DCC coupling of *tert*-butyldimethylsilyloxy-acetic acid[12] with 1,1′,2-trisnorsqualene alcohol (**6**) followed by nBu_4NF cleavage of the silyl protecting group.

NPs' Physico-chemical Characterization. *NPs' Formation and Stability.* Both SqPNG and SqPNG-pH compounds showed the capability to spontaneously self-assemble as NPs in water by nanoprecipitation from ethanolic solutions.

The SqPNG NPs' average diameter was 140 ± 10 nm with a very low polydispersity index of around ~0.1, and their *Z*-potential was about −50 mV. The NP suspensions, whatever their concentration (from 0.16 to 10 mg/mL), were found to be very stable in different storage conditions (*i.e.*, 2 weeks at 37 °C, several weeks at 25 °C, and more than 1 month at 4 °C; see Figure 1 in the Supporting Information). Moreover, after 7 months, NMR analysis of SqPNG NP suspensions (10 mg/mL) showed that the chemical structure of the derivative was still intact within the nanoparticles. The SqPNG-pH NPs showed a comparable average size and *Z*-potential (about 150 nm and −50 mV) with SqPNG NPs, but, despite a close chemical structure, they displayed a less remarkable stability, which lasted for only 7−8 days (see Figure 2 in the Supporting Information).

Similarly, we have constructed fluorescently labeled SqPNG NPs by solubilizing the fluorochrome cholesteryl-BODIPY (0.5 wt %) in the ethanolic solutions of either SqPNG or SqPNG-pH before nanoprecipitation in water; these fluorescent NPs were shown to be stable in water (see Figure 3 in the Supporting Information). In cell culture medium, however, due to the presence of serum proteins, the average diameter of the NPs increased by about 20 nm, being stable for the 24 h duration of the experiment (see Figure 4 in the Supporting Information), and the *Z*-potential rose to about −20 mV.

NPs' Morphological Analysis. Cryo transmission electron microscopy (CryoTEM) analysis was performed on a SqPNG NP suspension and revealed a spherical and regular shape of the NPs (Figure 1A). Further TEM analysis after freeze-fracture has allowed the investigation of the NPs' internal morphology. It was discovered that they did not display any supramolecular organization (Figure 1B). X-ray diffraction studies by SAXS and WAXS have also confirmed the absence of any crystal structure, contrary to previously synthesized squalenoylated gemcitabine and squalenoylated 2′,3′-dideoxycytidine (ddC) nanoassemblies.[13]

Molecular Modeling. Molecular modeling studies were undertaken on SqPNG and SqPNG-pH bioconjugates (compounds **1** and **2**) featuring double-ester arrangements as pro-drug interconnecting moieties.

The initial models were built using the ChemDraw structure of **1** and **2**, which were converted to 3D models using Chem3D software. These two models were initially energy-minimized *in vacuo* using the AM1[14] semiempirical method present in the HyperChem package and subsequently submitted to a sequence of 50 short molecular dynamics trajectories (10 ps under the molecular mechanics method OPLS, *i.e.*, optimized potentials

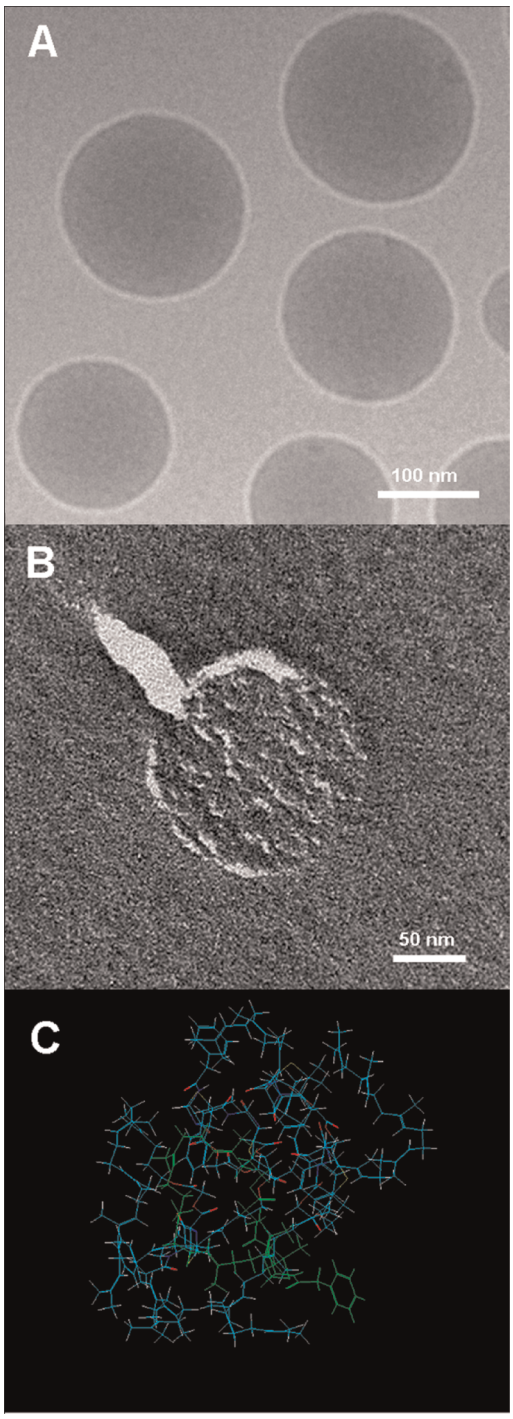

Figure 1. Morphological appearance of SqPNG NPs upon CryoTEM (A) and TEM after freeze-fracture (B). Results of energy minimization using the AM1 method on a stack of SqPNG molecules (C): total energy of the complete assembly ΔH = −1183.93 kcal/mol (AM1); energy of the selected (green) molecule ΔH = −193.44 kcal/mol (AM1); energy of the nonselected (blue) molecules ΔH = −979.95 kcal/mol (AM1); binding energy = total − Σ(partial)= −20.52 kcal/mol. To depict the conformation of a single SqPNG molecule, one molecule is shown in green.

for liquid simulations,[15] followed by energy minimization using the AM1 method in order to sample the conformational space of **1** and **2**). These calculations indicated that extended linear conformations of the squalene side chain were favored over conformers showing a bend somewhere along the lipophilic side chain.

For both **1** and **2**, the lowest ΔH linearly extended conformation models were selected for further studies. It should be noted at this stage that no significantly different ΔH values were obtained for **1** and **2**.

Duplex models of **1** and **2** were built by assembling the above selected conformers in a parallel or antiparallel mode. Using the same approach as for the single entities, it was found that the antiparallel mode was energy favored; this applied for both duplex 1:1 and duplex 2:2 models.

Finally, quintuplex models featuring 5 units of **1** or **2** were assembled using the antiparallel mode and were subjected to a sequence of 10 molecular dynamics trajectories (10 ps under molecular mechanics method OPLS) followed by energy minimization using the AM1 method. The lowest ΔH system was energy-analyzed as shown in Figure 1C.

The same process applied to quintuplex **1** gave a slightly lower (although statistically not significant) binding energy on the order of -15 ± 5 kcal/mol ($n = 10$) compared to 20 ± 5 kcal/mol ($n = 10$) for quintuplex **2**. This trend was difficult to further substantiate, although slight differences were found at the level of the electrostatic potential values of the heteroatoms, especially around the oxygen's double ester moieties.

As can be seen from inspection of these figures, the carbonyl double bonds of **1** were slightly more polarized than those of **2**.

In an effort to study the effect of water solvation, we examined also **1** and **2** in a periodic box of water molecules. Various attempts were made to evidence hydrogen bond formation between water and solutes **1** and **2**. In a very few frames, we were able to evidence a single hydrogen bond and this mainly at the level of the amide oxygen. This bond was also very weak. In other words, both **1** and **2** are highly lipophilic compounds, and within the nanoparticles formed by addition of either ethanolic solution of **1** or **2** to water, structuring by water as often observed previously is very unlikely. Clearly, these entities are mainly stabilized by strong hydrophobic forces.

Direct Antibacterial Activity of NPs. The antibacterial activity of SqPNG NPs was investigated against several bacterial strains, both sensitive and resistant to PNG. PNG and other β-lactam antibiotics prevent the interpeptidoglycan linkage of the bacterial wall, causing the arrest of bacterial multiplication.[16] The controlled and targeted release of PNG is therefore essential to prevent the extracellular release of low concentrations of antibiotic, leading to the emergence of bacterial resistance.[17−19]

TABLE 1. Minimum Inhibitory Concentration of PNG and SqPNG NPs in Several Bacterial Strains

	minimum inhibitory concentration (MIC)	
bacterial strain	penicillin G (μg/mL)	SqPNG NPs (μg/mL)
Enterococcus faecalis ATCC 29212	4	>128
Escherichia coli ATCC 8739	128	>128
Listeria monocytogenes ATCC 15313	>128	>128
Proteus vulgaris ATCC 13315	16	>128
Serratia marcescens ATCC 13880	>128	>128
Shigella sonnei ATCC 25931	64	>128
Staphylococcus aureus MRSA ATCC 33591	64	>128
Staphylococcus aureus ATCC 55585	0.03	2
Pseudomonas aeruginosa ATCC 9027	>128	>128
Streptococcus pneumoniae ATCC 33400	0.12	>128
Salmonella typhimurium ATCC 13311	2	>128
Streptococcus pyogenes ATCC 12344	0.06	16

We quantified the minimum inhibitory concentration for proliferation of bacteria (MIC) of free PNG and of SqPNG NPs. Results, reported in Table 1, clearly show the absence of any significant antibiotic activity of SqPNG NPs against all the tested strains except for *Staphylococcus aureus* and *Streptococcus pyogenes*, probably because PNG was not released from NPs in these experimental conditions.

Noteworthy, *Streptococcus pyogenes* ATCC 12344 and *Staphylococcus aureus* ATCC 55585 displayed high sensitivity toward PNG and NPs. To explain these results, it was calculated that if only about 4% of PNG release occurred, this would be enough to obtain a MIC of 16 μg/mL for *S. pyogenes* ATCC 12344 and 2 μg/mL for *S. aureus* ATCC 55585.

In the same way, SqPNG-pH NPs were tested against *S. aureus* ATCC 55585 and showed a lower MIC (0.125 μg/mL) than SqPNG NPs (2.00 μg/mL), although still higher than free PNG (0.03 μg/mL), probably due to the lower stability of SqPNG-pH compared with SqPNG, resulting in more PNG being released in the bacteria culture media after 18 h of incubation.

Uptake of NPs by J774 Cells. The ability of SqPNG and SqPNG-pH NPs to be internalized by macrophages was studied, using the cell line J774, a murine macrophage model commonly used.[20−22] In order to study the kinetics of the NP internalization, fluorescent BODIPY-cholesterol tagged NPs were incubated with J744 macrophages and cell fluorescence was analyzed by flow cytometry in comparison to untreated cells. We observed (Figure 2) that both types of NPs were internalized after 2 h of incubation; SqPNG reached a maximum at 6 h, while fluorescence of SqPNG-pH NPs continued to increase during the 24 h incubation

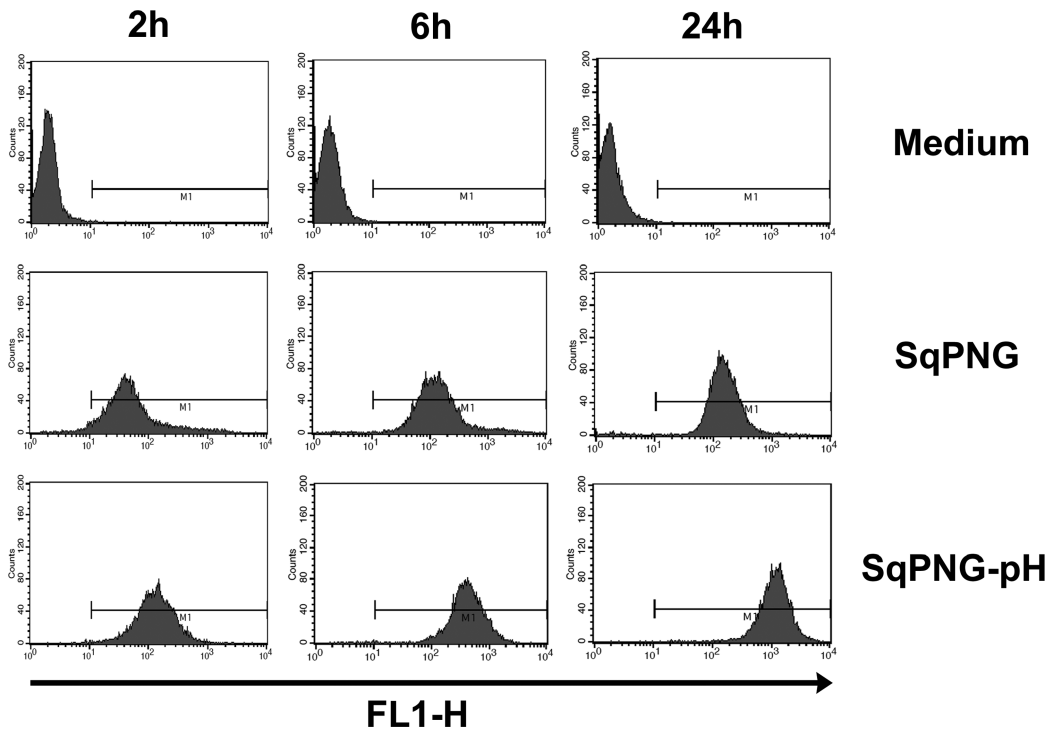

Figure 2. Kinetics of NP (either SqPNG or SqPNG-pH) internalization in J774 macrophages by flow cytometry. Cells were incubated with NPs during 2, 6, and 24 h in RPMI1640 + 0.5% v/v FBSd. The green fluorescence from BODIPY-labeled NPs was read in FL1-H.

[SqPNG: 6 h MFI = 130, 24 h MFI = 153; SqPNG-pH: 6 h MFI = 409, 24 h MFI = 1112 (MFI = mean fluorescence intensity)]. These results evidenced that NPs were differently internalized by macrophages depending on the linkage (*i.e.*, pH-sensitive or pH-insensitive) between squalene and PNG. Moreover, it was observed that NPs were also significantly internalized by PLB-985, a human myeloid cell line differentiated in neutrophil-like[23] (see Figure 5 in the Supporting Information). SqPNG-pH NP internalization was confirmed using confocal microscopy (Figure 6 in the Supporting Information). We can see pictures of the median plane of cells treated with SqPNG-pH fluorescent NPs; the observed green spots were clearly located in the cytosol. Moreover, we have performed an additional experiment using a membrane fluorescent marker (phycoerythrin-conjugated anti-CD11b, an antibody against CD11b coupled to phycoerythrin) to check if there is (or not) co-localization with the fluorescently labeled NPs. The results clearly indicated that the major fraction of the SqPNG-pH NPs was cell-internalized and not localized on the surface of the cell membrane (Figure 9 in the Supporting Information). The absence of fluorescence signals focused at the cell surface suggested that NPs of SqPNG-pH were internalized by the J774 macrophages and concentrated in intracellular compartments. These results are in accordance with the well-known macrophages' role in removal of NPs from the blood.[24]

Intracellular Bactericidal Effect of NPs. As *S. aureus* is known to invade and survive in macrophages,[25] based on the previous data (Table 1), the PNG-sensitive *S. aureus* ATCC 55585 strain was chosen as a model to study the intracellular bactericidal effect of the PNG-based NPs. Experimental conditions were chosen using a variant of the gentamicin protection assay, in order to keep only the intracellular bacteria alive while maintaining at least 95% of cell viability over the 24 h of the assay. This has been measured by trypan blue assay, since the MTT assay could not be performed with infected cells. Practically, cells were preincubated with different NP formulations maintaining similar PNG concentrations (20 μg/mL) and then infected with *S. aureus* bacteria for 2 h. After 6 h of treatment with gentamicin (to remove extracellular bacteria), we observed (Figure 3A) that control PNG-unloaded NPs (obtained by nanoprecipitation of the Sq-est 7) as well as free PNG had no antimicrobial activity on intracellular bacteria. On the contrary, both tested NPs displayed a significant effect in reducing the number of intracellular bacteria, which was more pronounced for the NPs with a pH-sensitive linker between squalene and penicillin G (*i.e.*, SqPNG-pH NPs induced a 78% decrease in viable intracellular bacteria). After 24 h of treatment with gentamicin, the bactericidal profile was slightly different. Indeed, free PNG induced a 56% decrease of bacterial viability, whereas SqPNG-pH NPs were still more effective in killing intracellular bacteria (*i.e.*, 87% reduction). As previously described,

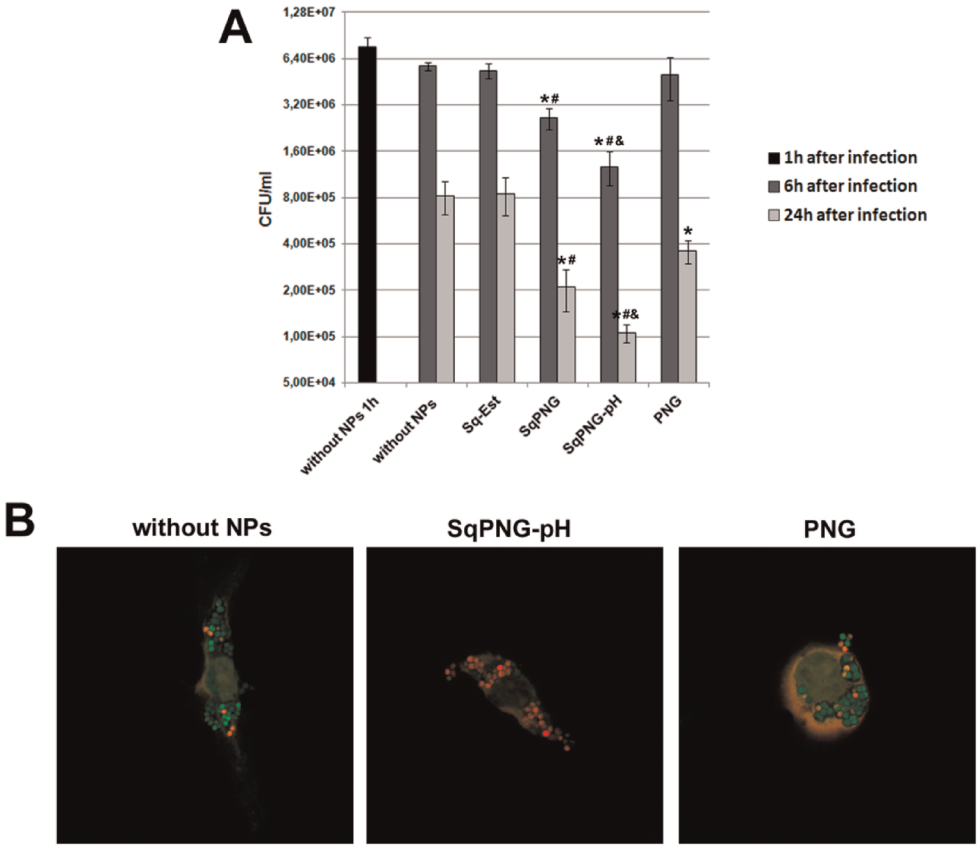

Figure 3. (A) CFU of intracellular *S. aureus* of cells treated with free PNG, SqPNG NPs, or SqPNG-pH NPs, all at 20 μg/mL equiv PNG (*i.e.*, 50 μg/mL total weight for the NP formulations). Experimental conditions: after treatment (6 h), J774 cells were washed and allowed to engulf *S. aureus* at a multiplicity of infection (MOI) of 10 for 2 h. To remove the extracellular bacteria, J774 macrophages were then washed again and incubated with gentamicin (50 μg/mL) during 1 (black), 6 (gray), or 24 (light gray) hours. Cell lysates were plated onto BHI/agar for CFU enumeration after 24 h. The data show three independent experiments (means $\pm$ SD). *$p < 0.05$ compared with "without NPs"; $^{\#}p < 0.05$ compared with PNG; $^{\&}p < 0.05$ compared with SqPNG. (B) Confocal fluorescence microscopy images of viable bacteria in J774 cells. J774 cells were pretreated with NPs then infected with *S. aureus* and fixed with paraformaldehyde, permeabilized with 0.2% Triton X-100, and double-labeled with propidium iodide and Syto9 (LIVE/DEAD BacLight kit). Viable *S. aureus* cells are stained in green, while red signals represent dead bacteria.

the decrease of the number of intracellular bacteria following free PNG treatment after 24 h hours may be explained by the cooperative effect of gentamicin and PNG allowing a small amount of PNG to indeed diffuse intracellularly.[17] The fact that there was no difference, after 6 h, in the intracellular bacterial counts between the untreated cells, the cells treated with the PNG-unloaded NPs (*i.e.*, Sq-Est), and the PNG incubated free clearly suggested that the pure squalene NPs (Sq-Est) did not induce any antibacterial effect and that free PNG had no intracellular bactericidal effect at this time point, likely because of insufficient diffusion into cells.[26] Our data clearly suggested that PNG NPs improved the cell penetration of the antibiotic, which allowed the rise of a significant bactericidal effect. Moreover, the better antibacterial activity of SqPNG-pH NPs *versus* SqPNG NPs may be reasonably explained by the acid-sensitive linkage in SqPNG-pH NPs, which could trigger a more efficient release of penicillin G in the cells.

We further investigated the influence of the different treatments on the intracellular bacterial viability by staining the bacteria with the LIVE/DEAD BacLight kit, which allowed to differentiate between live and dead *S. aureus* (by staining the latter with a red fluorophore and the viable bacteria with a green fluorophore)[27] (Figure 3B). Clearly, free PNG did not induce any significant mortality of intracellular *S. aureus*, unlike SqPNG-pH NPs, which gave rise to many red bacteria, the same ratio as colony-forming unit (CFU) enumeration.

It has, however, to be noted that if SqPNG-pH NPs showed a dramatic ability to kill most of the intracellular *S. aureus* (*i.e.*, 87%) in comparison with all the other treatments, they failed in killing all the intracellular bacteria after 24 h. This may be attributed either to insufficient intracellular PNG release from NPs to kill all bacteria or to the low metabolic state of a fraction of the intracellular bacteria, which may prevent an antibiotic effect,[26,28] or to both events. This deserves further investigations to further improve the antibiotic treatment toward these intracellular bacteria.

Mechanism of NP SqPNG-pH Internalization. Even though phagocytosis is a well-known uptake mechanism of

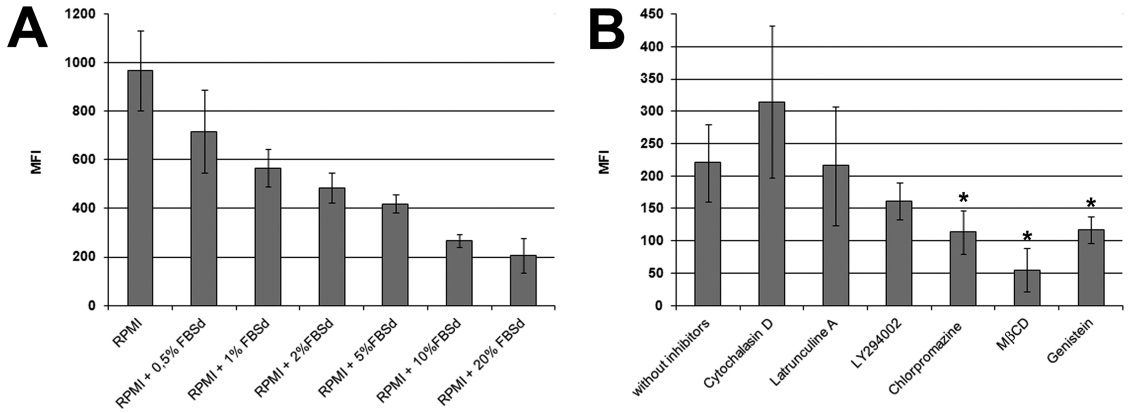

Figure 4. Influence of decomplemented fetal bovine serum (FBSd) on the internalization of SqPNG-pH NPs in J774 cells by flow cytometry. Cells were incubated with 100 μg/mL NPs during 6 h (A). Internalization in J774 cells of SqPNG-pH NPs in the presence of endocytosis inhibitors (flow cytometry). Cells were preincubated 1 h with or without inhibitors, then with 25 μg/mL of NPs during 6 h in RPMI1640 + 0.5% v/v FBS (B). The green fluorescence of cholesteryl-BODIPY in the NPs is read in FL1-H.

macrophages, these cells are also capable of clathrin-dependent or -independent endocytosis.[29,30] These different mechanisms impact the cell internalization kinetics and the intracellular trafficking of the NPs, both parameters that influence the effectiveness of the carried drug.

In the context of treating intracellular infections, targeting a subcellular compartment is a relevant goal to achieve since the co-localization of NPs with bacteria in the same intracellular compartments should enhance the local concentration of the delivered antibiotic and improve the efficiency.[31] To dissect the mechanism underlying NP internalization in our model, we used different pharmacologic inhibitors of endocytosis pathways[32] and observed by cytometry their effect on the internalization of SqPNG-pH NPs. We have also investigated the effect of decomplemented serum (FBSd) on the NP uptake, as serum contains several opsonins able to increase cell internalization (Figure 4A).

Interestingly, it was found that increasing the concentration of decomplemented fetal bovine serum (FBSd) induced a significant decrease in the NP cell capture. Since the complement activation, principally responsible for inducing phagocytosis of particles, was absent in our experimental conditions, it is likely that other proteins, including those with a dysopsonin activity, may adsorb onto the surface of SqPNG-pH NPs.[33] The plasma proteome is, indeed, expected to contain many proteins, and 50 have been identified in association with various NPs.[34−37] Dysopsonins such as albumin and some apolipoproteins are considered to promote prolonged circulation times of NPs in the blood.[38−40] It has been suggested that dysopsonins, naturally occurring substances that inhibit phagocytic ingestion, usually by altering the surface properties of the phagocyte or particle or both, thereby interfering with opsonization or altering the metabolic activity of the phagocyte, may regulate the uptake of NPs.[39] In our case, it is possible that the hydrophobicity and rigidity of SqPNG-pH NPs increased the amount of bounded proteins such as albumin, apolipoproteins, or fibrinogen.[24,41−44] This deserves, however, further experimental clarification.

Different inhibitors were used to inhibit various entrance routes for the NPs: (i) phagocytosis and macropinocytosis (cytochalasin D, latrunculin A, LY294002) and (ii) clathrin- (chlorpromazine) and (iii) clathrin-independent (methyl-β-cyclodextrin (MβCD), genistein) pathways. Figure 4B clearly shows that several endocytosis pathways, including clathrin endocytosis, coexist for SqPNG-pH NP internalization, as already shown before with other types of NPs.[45]

In a nutshell, the negative effect of the serum combined with the absence of influence of phagocytosis inhibitors on NP cell capture allowed us to conclude that J774 did not use the same pathway of internalization for pathogens and squalenoylated NPs.

Intracellular Localization of NPs *versus* Bacteria in J774. To investigate the intracellular distribution of NPs, SqPNG-pH NPs labeled with BODIPY-cholesterol were incubated with J774 macrophages for 6 h and then treated with LysoTracker, a marker of late endosomal and lysosomal vesicles (Figure 5A). Only a partial co-localization of NPs with the fluorescent lysosomal marker was observed, which correlated with our previous findings that NPs employed different endocytosis pathways for cell internalization.

In order to investigate if NPs located or not with intracellular bacteria, we stained *S. aureus* with a high concentration of propidium iodide (red), whereas NPs were tagged with BODIPY-cholesterol (green). Treated cells were then observed by confocal microscopy (Figure 5B). It was observed that NPs and *S. aureus* were found in different intracellular compartments.

The question that arises is how to explain the ability of SqPNG-pH NPs to kill intracellular bacteria (Figure 3), knowing that they distribute in different intracellular vesicles than bacteria (Figure 5B). The suggested

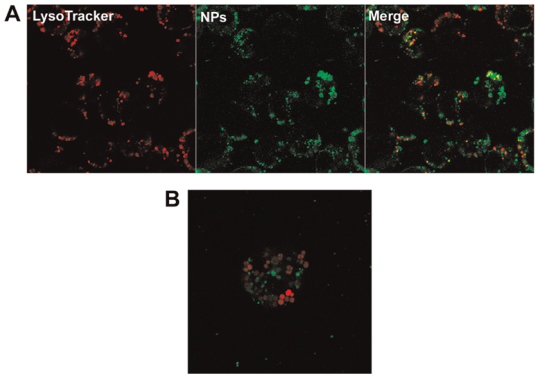

Figure 5. (A) J774 macrophages incubated with fluorescent SqPNG-pH NPs (green) at 6 h, then with LysoTracker Red DND-99 (40 nM) for 5 min and observed by confocal microscopy. Yellow color indicates the lysosomal localization of the NPs. (B) Localization of SqPNG-pH NPs and *S. aureus* ATCC55585 in J774 cells. J774 pretreated with fluorescent SqPNG-pH NPs (green) and then infected with stained IP *S. aureus* ATCC55585 (red) before fixation with paraformaldehyde (at 6 h post-treatment with gentamicin) and observed by confocal microscopy.

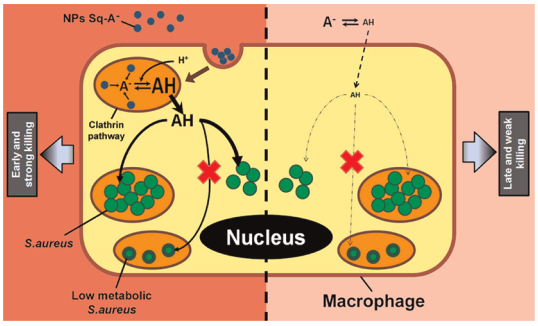

Figure 6. Schematic representation of the proposed mechanism of SqPNG-pH NP bactericidal activity inducing early and efficient killing of intracellular *S. aureus*.

mechanism results from the ability of PNG to cross the intracellular endolysosomal membranes after being released in the acidic environment of the lysosomes (Figure 5A).

As depicted in Figure 6, biological membranes are permeable only to the uncharged form of antibiotics. Thus, PNG, being a weak acid ($pK_a = 2.74$), is negatively charged (A^-) at neutral physiological pH. In this form, PNG cannot diffuse into the infected cells, which explains the poor antimicrobial activity of this antibiotic toward intracellular bacteria. The squalenoylated PNG-loaded nanoparticles did not follow this single-membrane diffusion process but entered into the cells through endocytotic pathways, including clathrin-dependent endocytosis, as demonstrated in this study (see Figure 4). Thus, SqPNG-pH NPs further accumulated in acidic late endosomes and lysosomes (different from bacterial ones), where their pH-sensitivity triggered the release of free PNG. In the acidic compartments, this antibiotic became protonated (AH) and therefore capable of crossing intracellular membranes and allowing further interaction with intracellular *S. aureus*.[46−48]

CONCLUSION

Two bioconjugates of penicillin G with squalene, using either a pH-sensitive (SqPNG-pH) or a pH-insensitive linker (SqPNG), were synthesized and found to spontaneously form stable nanoparticles.

The SqPNG-pH nanoparticles have proved to induce fast and significant killing of *S. aureus*-infected J774 cells. This approach opens interesting perspectives to combat invasive bacterial infections of macrophages such as *S. aureus*, which represents a worldwide public health concern and a major burden for the dairy industry.[25]

MATERIALS AND METHODS

Materials and Instrumentation. Penicillin G, squalene, and bromoacetic acid were purchased from Sigma-Aldrich Chemical Co., France. Phosphate-buffered solution (PBS) without $CaCl_2$ and $MgCl_2$, RMPI 1640 containing L-glutamine and 25 mM HEPES, and fetal bovine serum (FBS) were purchased from Dulbecco.

Propidium iodide was obtained from Invitrogen (Cergy-Pontoise, France). The following signaling inhibitors were obtained from Sigma: the tyrosine kinase inhibitor genistein, the phosphatidylinositol 3-kinase (PI3K) inhibitor LY-294002, the lipid raft-modifying drug methyl-β-cyclodextrin (MβCD), the clathrin endocytic pathway inhibitor chlorpromazine, and the actin cytoskeleton inhibitors cytochalasin D and latrunculine A. Cholesteryl BODIPY FL C12 (cholesteryl 4,4-difluoro-5,7-dimethyl-4 bora-3a,4°-diaza-5-indacene-3-dodecanoate) and LysoTracker Red DND-99 were Invitrogen Molecular Probes products. In all biological experiments, Milli-Q water (Millipore Synergy 185) was used. Other chemicals obtained from commercial suppliers were used without further purification.

IR spectra were obtained on solid or neat liquid on a Fourier transform Bruker Vector 22 spectrometer. Only significant absorptions are listed. Optical rotations were measured on a Perkin-Elmer 241 polarimeter at 589 nm. The ^1H and ^{13}C NMR spectra were recorded on a Bruker Avance 300 (300 and 75 MHz for ^1H and ^{13}C, respectively) or a Bruker Avance 400 (400 and 100 MHz for ^1H and ^{13}C, respectively) spectrometer. Recognition of methyl, methylene, methine, and quaternary carbon nuclei in ^{13}C NMR spectra rests on the *J*-modulated spin−echo sequence. Mass spectra were recorded on a Bruker Esquire-LC. Analytical thin-layer chromatography was performed on Merck silica gel $60F_{254}$ glass precoated plates (0.25 mm layer). Column chromatography was performed on Merck silica gel 60 (230−400 mesh ASTM). Diethyl ether and tetrahydrofuran (THF) were distilled from sodium/benzophenone ketyl. Methanol and ethanol were dried over magnesium and distilled. Benzene, toluene, DMF, and CH_2Cl_2 were distilled from calcium hydride, under a nitrogen atmosphere. All reactions involving air- or water-sensitive compounds were routinely conducted in glassware that was flame-dried under a positive pressure of nitrogen.

Synthesis of Bromoester (6). To a solution of 1,1′,2-trisnorsqualenyl alcohol **5** (500 mg, 1.3 mmol) in anhydrous CH_2Cl_2 (6 mL) was added bromoacetic acid (216 mg, 2.01 mmol) and 4-dimethylaminopyridine (DMAP) (10 mg, 0.08 mmol). The mixture was cooled to 0 °C, and DCC (317 mg, 1.95 mmol) was added portionwise. After being stirred at room temperature for 18 h, the reaction mixture was filtered through a cake of Celite. The solid was washed with a small amount of CH_2Cl_2.

The filtrate was concentrated under reduced pressure, and the residue was purified by chromatography on silica gel using elution with AcOEt/cyclohexane, 1:4. to give bromoester **6** as a colorless oil (460 mg, 70% yield). IR (neat, cm^{-1}): ν 2960−2850, 1739, 1700, 1448, 13821276, 1381. ^1H NMR (300 MHz, $CDCl_3$): δ 5.18−5.07 (m, 5 H), 4.14 (t, J = 6.4, 2 H), 3.82 (s, 2 H), 2.16−1.98 (m, 18 H), 1.70 (quint, J = 8.0 Hz, 2 H), 1.68 (s, 3 H), 1.53 (s, 15 H). ^{13}C NMR (75 MHz, $CDCl_3$): δ 167.2 (C), 135.0 (C), 134.8 (2C), 133.2 (C), 131.2 (C), 125.3 (CH), 124.4 (2 CH), 124.2 (2 CH), 65.9 (CH_2), 39.7 (2 CH_2), 39.6 (CH_2), 35.5 (CH_2), 28.2 (2 CH_2), 27.8 (CH_2), 26.6 (CH_2), 26.5 (2 CH_2),25.8 (CH_2), 25.6 (CH_3), 17.6 (CH_3), 16.0 (3 CH_3), 15.8 (CH_3).

Synthesis of Chloromethyl Ester (8). To a solution of 1,1′,2-trisnorsqualenic acid (**4**) (400 mg, 1.0 mmol) and n-Bu_4NHSO_4 (34 mg, 0.1 mmol) in CH_2Cl_2 (2 mL) was added a solution of $KHCO_3$ (300 mg, 3.0 mmol) in water (2 mL). The reaction mixture was vigorously stirred, and chloromethylsulfonyl chloride (185 mg, 1.15 mmol) was added dropwise. After being stirred for 1 h, CH_2Cl_2 (10 mL) was added. The organic phase was separated, washed with brine, dried over magnesium sulfate, and concentrated under reduced pressure to leave a pale yellow oil, which was used directly in the next step (382 mg, 81%). IR (neat, cm^{-1}): ν 2980−2845, 1768, 1710,1440, 1377, 1123, 1044. ^1H NMR ($CDCl_3$, 300 MHz): δ 5.69 (s, 1 H, OCH_2Cl), 5.20−5.00 (m, 5 H, HC═C(Me)), 2.60−2.40 (m, 2 H), 2.05−2.20 (m, 2H), 2.10−1.80 (m, 18 H), 1.68 (s, 3 H, C═$C(CH_3)_2$), 1.60 (s, 15 H, HC═$C(CH_3)$). ^{13}C NMR ($CDCl_3$, 100 MHz): δ 171.3 (C, CO_2), 135.1 (C), 134.9 (C), 134.8 (C), 132.5 (C), 131.2 (C), 125.6 (CH), 124.4 (CH), 124.4 (CH), 124.2 (2CH), 68.5 (CH_2, OCH_2Cl), 39.7 (2 CH_2), 39.5 (CH_2), 34.1 (CH_2), 32.8 (CH_2), 28. (2CH_2), 26.7 (CH_2), 26.6 (CH_2), 26.5 (CH_2), 25.7 (CH_3), 17.6 (CH_3), 16.0 (3CH_3), 15.9 (CH_3). MS (+APCI): m/z 449.3 (100%) $[M + H]^+$.

Synthesis of Squalenyl Conjugates. (SqPNG) (**1**): A mixture of penicillin G sodium salt (50 mg, 0.15 mmol) and 1,1′,2-trisnorsqualenyl bromoacetate (**3**) (113 mg, 0.22 mmol) in dry DMF (0.75 mL) was stirred at room temperature for 48 h. The reaction mixture was then concentrated under reduced pressure (0.05 Torr), and the residue was purified by chromatography on silica gel eluting with AcOEt/cyclohexane, 1:4, to give the bioconjugate **1** as a colorless, viscous oil (58 mg, 56% yield). $[\alpha]_D$ = +213.3 (EtOH, c 0.45). IR (neat, cm^{-1}): ν 3400−3100, 2931, 2854, 1789, 1753, 1691, 1659, 1495, 1453, 1375, 1295, 1199, 1177, 1152, 1130, 1075,1028. ^1H NMR (400 MHz, $CDCl_3$): δ 7.42−7.20 (m, 5 H), 6.10 (d, J = 9.1 Hz, 1 H, CONH), 5.65 (dd, J = 9.1, 4.2 Hz, 1 H, H-6), 5.50 (d, J = 4.2 Hz, 1 H, H-5), 5.20−5.10 (m, 5 H, HC═$C(CH_3)$), 4.75 (d, J = 15.8 Hz, 1 H, OCH_2CO_2), 4.58 (d, J = 15.8 Hz, 1 H, OCH_2CO_2), 4.43 (s, 1 H, H-2), 4.13 (t, J = 6.7 Hz, 2 H, $CO_2CH_2CH_2$), 3.63 (s, 2 H, $PhCH_2CO$), 2.12−1.92 (m, 18 H), 1.73 (quint, J = 8.0 Hz, 2 H), 1.68 (s, 3 H, C═$C(CH_3)_2$), 1.60 (s, 15 H, C═$C(CH_3)$), 1.57 (s, 3 H, $SC(CH_3)_2$), 1.50 (s, 3 H, $SC(CH_3)_2$). ^{13}C NMR (100 MHz, $CDCl_3$): δ 173.7 (C, CO), 170.3 (C, CO), 167.0 (C, CO), 166.9 (C, CO), 135.1 (C), 134.9 (C), 133.8 (C), 133.2 (C), 131.2 (C), 129.5 (2CH), 129.1 (2CH), 127.6 (CH), 125.4 (CH), 124.4 (2 CH), 124.2 (2CH), 70.3 (CH, C-2), 67.9 (CH, C-5), 65.4 (CH_2, $CO_2CH_2CH_2$), 64.6 (C, C-3,), 61.2 (CH_2, OCH_2CO_2), 58.5 (CH, C-6), 43.3 (CH_2, $PhCH_2$), 39.7 (CH_2), 39.6 (CH_2), 35.5 (CH_2), 31.1 (CH_3, $SC(CH_3)_2$), 28.2 (3 CH_2), 26.7 (CH_3), 26.7 (CH_2), 26.6 (3 CH_2), 25.7 (CH_3), 17.7 (CH_3), 16.0 (3 CH_3), 15.8 (CH_3). MS (-APCI): m/z (%) 760 (100) $[M - H]^-$.

(SqPNG-pH) (**2**): A mixture of penicillin G sodium salt (180 mg, 0.50 mmol) and trisnorsqualenic acid chloromethyl ester (**8**) (230 mg, 0.51 mmol) in DMF (3 mL) was stirred at room temperature for 4 d. The reaction mixture was concentrated under reduced pressure, and the residue was taken into water. The mixture was extracted with CH_2Cl_2. The combined organic extracts were washed with brine, dried over $MgSO_4$, and concentrated under reduced pressure. Chromatographic purification on silica gel eluting with cyclohexane/AcOEt, 4:1, afforded conjugate **2** as a colorless oil (182 mg, 49%). $[\alpha]_D$ = +137.4 (EtOH, c 1.4). IR (neat, cm^{-1}): ν 3034, 2927, 2851, 1792, 1768, 1738, 1678, 1451, 1373, 1296, 1241, 1116, 1046, 985, 909. ^1H NMR ($CDCl_3$, 300 MHz): δ 7.40−7.25 (m, 5 H, Ph), 6.07 (br s, 1 H, NH), 5.80 (d, J = 5.5 Hz, 1 H, OCH_2O), 5.74 (d, J = 5.5 Hz, 1 H, OCH_2O), 5.65 (dd, J = 9.1 Hz, J = 4.2 Hz, 1 H, H-6), 5.49 (d, d, J = 4.3 Hz, 1 H, H-5), 5.20−5.02 (m, 5 H, HC═$C(CH_3)$), 4.38 (s, 1 H, H-2), 3.63 (s, 2 H, $PhCH_2$), 2.48−2.40 (m, 2 H, $COCH_2CH_2$), 2.30−2.25 (m, 2 H, $COCH_2CH_2$), 2.14−1.90 (m, 16 H, ═$CHCH_2CH_2C(CH_3)$), 1.68 (s, 3 H, $(CH_3)_2C$═), 1.58 (s, 15 H, CH_3), 1.44 (s, 3 H, $C(CH_3)_2$), 1.43 (s, 3 H, $C(CH_3)_2$). ^{13}C NMR ($CDCl_3$, 100 MHz): δ 173.4 (C, CO), 171.7 (C, CO), 170.3 (C, CO), 166.3 (C, CO), 135.1 (C, ═$C(CH_3)$), 134.8 (C, ═$C(CH_3)$), 134.7 (C, ═$C(CH_3)$), 133.7 (C, Ph), 132.5 (C, ═$C(CH_3)$), 131.2 (C, ═$C(CH_3)_2$), 129.5 (2CH, Ph), 129.1 (2CH, Ph), 127.6 (CH, Ph), 125.5 (CH, HC═$C(CH_3)$), 124.4 (CH, HC═$C(CH_3)$), 124.3 (CH, HC═$C(CH_3)$), 124.2 (2CH, HC═$C(CH_3)$), 79.5 (CH_2, OCH_2O), 69.9 (CH, C-2), 68.0 (CH, C-5), 64.4 (C, C-3), 58.8 (CH, C-6), 43.3 (CH_2, $PhCH_2$), 39.7 (2 CH_2, ═$C(CH_3)CH_2$), 39.4 (CH_2, ═$C(CH_3)CH_2$), 34.0 (CH_2, $COCH_2CH_2$), 32.7 (CH_2, $COCH_2CH_2$), 31.6 (CH_3, $SC(CH_3)_2$), 28.2 (2CH_2, ═$CHCH_2$),), 26.7 (CH_2, ═$CHCH_2$),), 26.6 (CH_2, ═$CHCH_2$), 25.6 (2CH_3, ═$C(CH_3)_2$, $SC(CH_3)_2$), 17.6 (CH_3), 16.0 (3CH_3), 15.8 (CH_3). MS (+APCI): m/z 747.5 (30) $[M + H]^+$; 721.5 (100), 572.4 (40) $[M - PhCH_2CH$═C═$O + H]^+$.

NP Formation, Characterization, and Stability. In a typical procedure, 4 mg of SqPNG or 4 mg of SqPNG-pH was dissolved in 0.5 mL of ethanol and added dropwise to 1 mL of distilled water, giving rise to the spontaneous formation of nanoparticles. Ethanol was then evaporated under vacuum using a Rotavapor to obtain an aqueous suspension of SqPNG or SqPNG-pH NPs.

Similarly, Sq-Est (**7**) NPs were obtained using the same procedure as described above for SqPNG and SqPNG-pH derivatives. Sq-Est NPs were used as negative control in antibacterial tests.

In order to check the absence of free, nonassembled SqPNG or SqPNG-pH conjugates in solution, SqPNG and SqPNG-pH NPs were ultracentrifugated at 40 000 rpm for 120 min, and the supernatant was analyzed by HPLC (H5C18-25 M INTERCHROM C18 Hypersil 5 μm, 250 × 4,6 mm column, eluent CH_3OH/H_2O, 95:5, λ_1 = 208 nm and λ_2 = 260 nm); for both SqPNG and SqPNG-pH, less than 1% was found free in the supernatant.

The size and the polydispersity of NPs at various dilutions and in different storage conditions (in suspension in water at 4, 25, and 37 °C, and in RPMI medium at 37 °C) were determined at 20 °C by quasi-elastic light scattering using a nanosizer (Zetasizer Nano 6.12, Malvern Instruments Ltd., UK). The selected angle was 173°, and the measurement was made after dilution to 1:25 of the NP suspension in Milli-Q water. The Z-potential was determined using a Zetasizer (Zetasizer 4, Malvern Instruments Ltd., UK), after dilution of 1 mL of the NPs suspension in 1 mL of KCl (1 mM).

Preparation of Fluorescent NPs. Fluorescently labeled NPs were obtained by nanoprecipitation in water of an ethanolic solution of SqPNG or SqPNG-pH (4 mg/mL) containing 0.5% w/w of the hydrophobic green dye cholesteryl BODIPY FL C12. The solvent was then evaporated under vacuum; the centrifugation of fluorescent NPs and the spectrofluorimetric analysis of the supernatant showed the absence of free fluorochrome in solution, showing that cholesteryl BODIPY FL C12 was associated with PNG NPs. In further experiments, fluorescent NPs were not ultracentrifuged, and the size and polydispersity were determined in different storage conditions (*i.e.*, NP suspension in water at 4 °C or in RPMI 5% FBSd at 37 °C).

Cryogenic Transmission Electron Microscopy. The morphology of SqPNG NPs was investigated by cryogenic transmission electron microscopy analysis or by transmission electron microscopy after freeze-fracture (FFTEM).

For CryoTEM, 4 μL of a concentrated SqPNG NPs suspension (10 mg/mL) was deposited onto a perforated carbon film mounted on a 200 mesh electron microscopy grid. The homemade carbon film hole dimensions were about 2 mm in diameter. Most of the drop was removed with a blotting filter paper, and the residual thin films remaining within the holes were vitrified after immersion in liquid ethane using a guillotine-like frame. The specimen was then transferred, using liquid nitrogen, to a cryospecimen holder and observed using a JEOL FEG-2010 electron microscope. Micrographs were recorded at 200 kV under low-dose conditions at a magnification of 40 000 on SO-163 Kodak film. Micrographs were digitized using a film scanner (Super Coolscan 8000 ED, Nikon), and analysis was made using ImageJ software.

For FFTEM observations, a drop of the sample was placed on a copper support, immediately frozen in liquid propane, and then kept in liquid nitrogen. Fracturing and shadowing were performed in a Balzers BAF 400 freeze-etching unit. The replicas were washed in THF and in distilled water and placed on copper grids. Observations were made under a TEM JEOL 100SX.

Antibacterial Activity of the NPs. The antibacterial activity of SqPNG NPs was investigated against several bacterial strains, both sensitive and resistant to penicillin G. The antibacterial activities were carried out in a quantitative assay based on dilution method, using Mueller-Hinton medium (with 10% v/v of FBSd when needed), and the MIC was determined for SqPNG NPs, SqPNG-pH, and free PNG as positive control.

The analysis was conducted preparing various dilutions of penicillin G and NPs from 128 to 0.015 μg/mL in different test tubes (final volume 1 mL) inoculated with equal quantities of bacterial culture (5×10^5 bacteria/mL). After incubation at 37 °C for 18 h, the turbidity of the solutions was examined. The first test tube, in dilution order, which presented a clear solution, was that which contained the minimum inhibitory concentration of the antibiotic. Results were also confirmed by bacterial plating on agar.

Macrophage Cell Line. The J774 murine cell line was used as macrophage model. The cells were grown in RPMI-1640 medium (BioWhittaker, Walkerville, MD, USA) supplemented with 10% v/v fetal bovine decomplemented serum (Cambrex BioSciences, Verviers, Belgium) at 37 °C in humidified air containing 5% CO_2. The cells were scraped to avoid cell confluence.

Bacterial Culture. The penicillin-sensitive *S. aureus* (strain ATCC55585) stock cultures were maintained in 20% glycerol at −80 °C. Before experiments, the bacteria were transferred onto fresh brain heart infusion (BHI)/agar (Difco, Invitrogen, Cergy-Pontoise, France) and incubated at 37 °C for 24 h. For each experiment, bacteria were subcultured in BHI (medium) at 37 °C for 18 h. The day of the experiment, the bacteria were washed twice with sterile PBS, counted in a Salumbini chamber, and adjusted to 1×10^7 bacteria/mL in RPMI-1640 medium supplemented with 10% v/v FBSd.

NP Internalization in J774 Cells. About 5×10^5 J774 cells were put on 24-well tissue-culture plates with (for microscopy) or without (cytometry) glass coverslips and incubated during the night (around 12 h) at 37 °C in humidified air containing 5% CO_2 to ensure cell adherence. Cells were then washed with RPMI 1640 + 0.5% v/v FBSd and incubated with 100 μg/mL of the different fluorescent NPs (*i.e.*, SqPNG or SqPNG-pH) in RPMI 1640 with 0.5% v/v FBSd during 2, 6, and 24 h (37 °C, 5% CO_2). Different concentrations of FBSd (0.5%, 1%, 2%, 5%, 10%, 20%) in the cell culture medium have been used to study the influence of decomplemented serum on the cell internalization of SqPNG-pH NPs (incubation time of 6 h). Different pharmacological inhibitors (cytochalasin D 5 μg/mL, latrunculine A 100 nM, LY294002 25 μM, chlorpromazine 25 μM, MβCD 2 mM, genistein 100 μM) have also been used to investigate NPs' phagocytotic/endocytotic pathways.[32] Practically, the cells were preincubated 1 h with one of the above-mentioned inhibitors before further incubation (6 h) with SqPNG-pH NPs (at 25 μg/mL in RPMI 1640 with 0.5% v/v FBSd at 37 °C and 5% CO_2). For flow cytometry, cells were washed with PBS and then treated with 0.25% trypsin for 10 min at 37 °C and 5% CO_2. Afterward, cells were vigorously dispersed and washed with RPMI 1640 + 10% FBSd. After centrifugation at 1500 rpm for 5 min in cytometry tubes, cells were resuspended with 400 μL of a solution of paraformaldehyde (PFA) 1% w/v in PBS and kept on ice until flow cytometry. A FACSCalibur flow cytometer equipped with a 15 mV, 488 nm argon laser (Becton Dickinson, San Jose, CA, USA) was used. The data were analyzed with CellQuest software. Fluorescence was recorded with a constant photomultiplier gain, and the results were expressed as the mean fluorescence intensity on a four-decade logarithmic scale.

Intracellular Antimicrobial Activity of NPs. *Nanoparticle Incubation Step.* About 5×10^5 J774 cells were incubated on 24-well tissue-culture plates during the night (around 12 h) at 37 °C in humidified air containing 5% CO_2 to ensure cell adherence. The next day, cells were washed with RPMI 1640 + 0.5% v/v FBSd and then incubated for 6 h in the same cell culture medium (37 °C, 5% CO_2) with or without different treatments (*i.e.*, 20 μg/mL of PNG, 50 μg/mL of SqPNG, which was equivalent to 20 μg/mL PNG or 50 μg/mL SqPNG-pH NPs, also equivalent to 20 μg/mL of PNG). Squalene-ester NPs (Sq-Est) (50 μg/mL) were used as control in the same conditions.

S. aureus Infection Step. After NP treatment cells were washed twice with 1 mL of RPMI 1640 + 10% v/v FBSd in order to eliminate extracellular NPs and free PNG. Then, 500 μL of *S. aureus* suspension (ATCC55585) in the same medium was added at 10^7 bacteria/mL (multiplicity of infection, MOI = 10) and incubated for 2 h (37 °C, 5% CO_2). To remove nonphagocytosed bacteria, J774 cells were washed and any extracellular bacteria were killed by further incubation in RPMI 1640 medium containing gentamicin (50 μg/mL). After 1, 6, and 24 h of incubation, cells were washed again with RPMI 1640 + 10% v/v FBSd and lysed by treatment with ice-cold water during 1 h. The lysates were plated at serial dilutions in sterile PBS on BHI/agar plates. The plates were incubated at 37 °C overnight, and the number of formed colonies was evaluated following the usual methodologies.[27,49,50]

For confocal microscopy studies, J774 cells were treated then infected in similar conditions as explained previously. Thereafter, the cells were washed with 1 mL of PBS, fixed with 1% PFA, and permeabilized with 0.2% Triton-X100. They were then brought into the mix of the LIVE/DEAD BacLight bacterial viability kit (Molecular Probes) for 15 min in the dark.[27] After washing with 1 mL of PBS, J774 cells were observed with an inverted Zeiss (Jena, Germany) LSM-510 META confocal laser scanning microscope.

Localization of NPs. For intracellular localization studies, 5×10^5 cells were treated with fluorescent NPs for 6 h, washed with PBS, and incubated with 1 mL of LysoTracker Red DND-99 solution (40 nM)[51] in RPMI medium (5 min at 37 °C, 5% CO_2). After washing, the coverslips were mounted and the fluorescence was immediately examined with an inverted Zeiss (Jena, Germany) LSM-510 META confocal laser scanning microscope equipped with an argon laser and helium neon laser (Plan-Apochromat 63× objective lens NA 1.40, oil immersion).

To visualize *S. aureus* in confocal microscopy, bacteria were incubated for 1 h at 37 °C with a high concentration of IP and washed three times with PBS before the infection step was performed as explained before. After 6 h of incubation with gentamicin, cells were washed three times with PBS, then fixed with 3% PFA at room temperature for 15 min. The washed coverslips were mounted, and the fluorescence was examined with an inverted Zeiss (Jena, Germany) LSM-510 META confocal laser scanning microscope.

Conflict of Interest: The authors declare no competing financial interest.

Acknowledgment. The research leading to these results has received funding from the European Research Council under the European Community's Seventh Framework Programme FP7/2007-2013 (grant agreement no. 249835).

Supporting Information Available: Detailed experimental section [PLB-985 culture; cytotoxicity assay; localization of NPs compared to CD11b membrane], supporting references, and supporting Figures S1 to S9. This material is available free of charge *via* the Internet at http://pubs.acs.org.

REFERENCES AND NOTES

1. Laskay, T.; van Zandbergen, G.; Solbach, W. Neutrophil Granulocytes--Trojan Horses for Leishmania Major and Other Intracellular Microbes? *Trends Microbiol.* **2003**, *11*, 210–214.
2. Abeylath, S. C.; Turos, E. Drug Delivery Approaches to Overcome Bacterial Resistance to Beta-Lactam Antibiotics. *Expert Opin. Drug Delivery* **2008**, *5*, 931–949.
3. Pinto-Alphandary, H.; Andremont, A.; Couvreur, P. Targeted Delivery of Antibiotics Using Liposomes and Nanoparticles: Research and Applications. *Int. J. Antimicrob. Agents* **2000**, *13*, 155–168.
4. Drulis-Kawa, Z.; Dorotkiewicz-Jach, A. Liposomes as Delivery Systems for Antibiotics. *Int. J. Pharm.* **2010**, *387*, 187–198.
5. Pinto-Alphandary, H.; Balland, O.; Laurent, M.; Andremont, A.; Puisieux, F.; Couvreur, P. Intracellular Visualization of Ampicillin-Loaded Nanoparticles in Peritoneal Macrophages Infected *in Vitro* with *Salmonella Typhimurium*. *Pharm. Res.* **1994**, *11*, 38–46.

6. Forestier, F.; Gerrier, P.; Chaumard, C.; Quero, A. M.; Couvreur, P.; Labarre, C. Effect of Nanoparticle-Bound Ampicillin on the Survival of Listeria Monocytogenes in Mouse Peritoneal Macrophages. *J. Antimicrob. Chemother.* **1992**, *30*, 173–179.
7. Couvreur, P.; Stella, B.; Reddy, L. H.; Hillaireau, H.; Dubernet, C.; Desmaele, D.; Lepetre-Mouelhi, S.; Rocco, F.; Dereuddre-Bosquet, N.; Clayette, P.; *et al*. Squalenoyl Nanomedicines as Potential Therapeutics. *Nano Lett.* **2006**, *6*, 2544–2548.
8. Sen, S. E.; Prestwich, G. D. Squalene Analogues Containing Isopropylidene Mimics as Potential Inhibitors of Pig Liver Squalene Epoxidase and Oxidosqualene Cyclase. *J. Med. Chem.* **1989**, *32*, 2152–2158.
9. Daehne, W.; Frederiksen, E.; Gundersen, E.; Lund, F.; Morch, P.; Petersen, H. J.; Roholt, K.; Tybring, L.; Godtfredsen, W. O. Acyloxymethyl Esters of Ampicillin. *J. Med. Chem.* **1970**, *13*, 607–612.
10. Jansen, A. B.; Russell, T. J. Some Novel Penicillin Derivatives. *J. Chem. Soc.* **1965**, *65*, 2127–2132.
11. Baltzer, B.; Binderup, E.; von Daehne, W.; Godtfredsen, W. O.; Hansen, K.; Nielsen, B.; Sorensen, H.; Vangedal, S. Mutual Pro-Drugs of Beta-Lactam Antibiotics and Beta-Lactamase Inhibitors. *J. Antibiot. (Tokyo)* **1980**, *33*, 1183–1192.
12. Klein, L. L.; Yeung, C. M.; Kurath, P.; Mao, J. C.; Fernandes, P. B.; Lartey, P. A.; Pernet, A. G. Synthesis and Activity of Nonhydrolyzable Pseudomonic Acid Analogues. *J. Med. Chem.* **1989**, *32*, 151–160.
13. Couvreur, P.; Reddy, L. H.; Mangenot, S.; Poupaert, J. H.; Desmaele, D.; Lepetre-Mouelhi, S.; Pili, B.; Bourgaux, C.; Amenitsch, H.; Ollivon, M. Discovery of New Hexagonal Supramolecular Nanostructures Formed by Squalenoylation of an Anticancer Nucleoside Analogue. *Small* **2008**, *4*, 247–253.
14. Dewar, M. J.; Storch, D. M. Alternative View of Enzyme Reactions. *Proc. Natl. Acad. Sci. U. S. A.* **1985**, *82*, 2225–2229.
15. Jorgensen, J. H.; Swenson, J. M.; Tenover, F. C.; Barry, A.; Ferraro, M. J.; Murray, P. R.; Reller, L. B. Development of Interpretive Criteria and Quality Control Limits for Macrolide and Clindamycin Susceptibility Testing of *Streptococcus Pneumoniae*. *J. Clin. Microbiol.* **1996**, *34*, 2679–2684.
16. Holten, K. B.; Onusko, E. M. Appropriate Prescribing of Oral Beta-Lactam Antibiotics. *Am. Fam. Physician* **2000**, *62*, 611–620.
17. Briones, E.; Colino, C. I.; Lanao, J. M. Delivery Systems to Increase the Selectivity of Antibiotics in Phagocytic Cells. *J. Controlled Release* **2008**, *125*, 210–227.
18. Hamilton-Miller, J. M. Antibiotic Resistance from Two Perspectives: Man and Microbe. *Int. J. Antimicrob. Agents* **2004**, *23*, 209–212.
19. Martinez, J. L.; Fajardo, A.; Garmendia, L.; Hernandez, A.; Linares, J. F.; Martinez-Solano, L.; Sanchez, M. B. A Global View of Antibiotic Resistance. *FEMS Microbiol. Rev.* **2009**, *33*, 44–65.
20. Balland, O.; Pinto-Alphandary, H.; Pecquet, S.; Andremont, A.; Couvreur, P. The Uptake of Ampicillin-Loaded Nanoparticles by Murine Macrophages Infected with *Salmonella Typhimurium*. *J. Antimicrob. Chemother.* **1994**, *33*, 509–522.
21. Balland, O.; Pinto-Alphandary, H.; Viron, A.; Puvion, E.; Andremont, A.; Couvreur, P. Intracellular Distribution of Ampicillin in Murine Macrophages Infected with *Salmonella Typhimurium* and Treated with (3h)Ampicillin-Loaded Nanoparticles. *J. Antimicrob. Chemother.* **1996**, *37*, 105–115.
22. Lemarchand, C.; Gref, R.; Passirani, C.; Garcion, E.; Petri, B.; Muller, R.; Costantini, D.; Couvreur, P. Influence of Polysaccharide Coating on the Interactions of Nanoparticles with Biological Systems. *Biomaterials* **2006**, *27*, 108–118.
23. Semiramoth, N.; Gleizes, A.; Turbica, I.; Sandre, C.; Marin-Esteban, V.; Gorges, R.; Servin, A.; Chollet-Martin, S. Afa/Dr-Expressing, Diffusely Adhering *Escherichia Coli* Strain C1845 Triggers F1845 Fimbria-Dependent Phosphatidylserine Externalization on Neutrophil-Like Differentiated Plb-985 Cells through an Apoptosis-Independent Mechanism. *Infect. Immun.* **2010**, *78*, 2974–2983.
24. Owens, D. E., 3rd; Peppas, N. A. Opsonization, Biodistribution, and Pharmacokinetics of Polymeric Nanoparticles. *Int. J. Pharm.* **2006**, *307*, 93–102.
25. Garzoni, C.; Kelley, W. L. *Staphylococcus Aureus*: New Evidence for Intracellular Persistence. *Trends Microbiol.* **2009**, *17*, 59–65.
26. Barcia-Macay, M.; Seral, C.; Mingeot-Leclercq, M. P.; Tulkens, P. M.; Van Bambeke, F. Pharmacodynamic Evaluation of the Intracellular Activities of Antibiotics against *Staphylococcus Aureus* in a Model of Thp-1 Macrophages. *Antimicrob. Agents Chemother.* **2006**, *50*, 841–851.
27. Kubica, M.; Guzik, K.; Koziel, J.; Zarebski, M.; Richter, W.; Gajkowska, B.; Golda, A.; Maciag-Gudowska, A.; Brix, K.; Shaw, L.; *et al*. A Potential New Pathway for *Staphylococcus Aureus* Dissemination: The Silent Survival of *S. Aureus* Phagocytosed by Human Monocyte-Derived Macrophages. *PLoS One* **2008**, *3*, e1409.
28. Melter, O.; Radojevic, B. Small Colony Variants of *Staphylococcus Aureus*--Review. *Folia Microbiol. (Praha)* **2010**, *55*, 548–558.
29. Kiss, A. L.; Geuze, H. J. Caveolae Can Be Alternative Endocytotic Structures in Elicited Macrophages. *Eur. J. Cell Biol.* **1997**, *73*, 19–27.
30. Perry, D. G.; Daugherty, G. L.; Martin, W. J., 2nd Clathrin-Coated Pit-Associated Proteins Are Required for Alveolar Macrophage Phagocytosis. *J. Immunol.* **1999**, *162*, 380–386.
31. Rajendran, L.; Knolker, H. J.; Simons, K. Subcellular Targeting Strategies for Drug Design and Delivery. *Nat. Rev. Drug Discovery* **2010**, *9*, 29–42.
32. Ivanov, A. I. Pharmacological Inhibition of Endocytic Pathways: Is It Specific Enough to Be Useful? *Methods Mol. Biol.* **2008**, *440*, 15–33.
33. Aggarwal, P.; Hall, J. B.; McLeland, C. B.; Dobrovolskaia, M. A.; McNeil, S. E. Nanoparticle Interaction with Plasma Proteins as It Relates to Particle Biodistribution, Biocompatibility and Therapeutic Efficacy. *Adv. Drug Delivery Rev.* **2009**, *61*, 428–437.
34. Dobrovolskaia, M. A.; Patri, A. K.; Zheng, J.; Clogston, J. D.; Ayub, N.; Aggarwal, P.; Neun, B. W.; Hall, J. B.; McNeil, S. E. Interaction of Colloidal Gold Nanoparticles with Human Blood: Effects on Particle Size and Analysis of Plasma Protein Binding Profiles. *Nanomedicine* **2009**, *5*, 106–117.
35. Goppert, T. M.; Muller, R. H. Protein Adsorption Patterns on Poloxamer- and Poloxamine-Stabilized Solid Lipid Nanoparticles (Sln). *Eur. J. Pharm. Biopharm.* **2005**, *60*, 361–372.
36. Kim, H. R.; Andrieux, K.; Delomenie, C.; Chacun, H.; Appel, M.; Desmaele, D.; Taran, F.; Georgin, D.; Couvreur, P.; Taverna, M. Analysis of Plasma Protein Adsorption onto Pegylated Nanoparticles by Complementary Methods: 2-De, Ce and Protein Lab-on-Chip System. *Electrophoresis* **2007**, *28*, 2252–2261.
37. Thode, K.; Luck, M.; Semmler, W.; Muller, R. H.; Kresse, M. Determination of Plasma Protein Adsorption on Magnetic Iron Oxides: Sample Preparation. *Pharm. Res.* **1997**, *14*, 905–910.
38. Goppert, T. M.; Muller, R. H. Adsorption Kinetics of Plasma Proteins on Solid Lipid Nanoparticles for Drug Targeting. *Int. J. Pharm.* **2005**, *302*, 172–186.
39. Moghimi, S. M.; Muir, I. S.; Illum, L.; Davis, S. S.; Kolb-Bachofen, V. Coating Particles with a Block Co-Polymer (Poloxamine-908) Suppresses Opsonization but Permits the Activity of Dysopsonins in the Serum. *Biochim. Biophys. Acta* **1993**, *1179*, 157–165.
40. Ogawara, K.; Furumoto, K.; Nagayama, S.; Minato, K.; Higaki, K.; Kai, T.; Kimura, T. Pre-Coating with Serum Albumin Reduces Receptor-Mediated Hepatic Disposition of Polystyrene Nanosphere: Implications for Rational Design of Nanoparticles. *J. Controlled Release* **2004**, *100*, 451–455.
41. Cedervall, T.; Lynch, I.; Lindman, S.; Berggard, T.; Thulin, E.; Nilsson, H.; Dawson, K. A.; Linse, S. Understanding the Nanoparticle-Protein Corona Using Methods to Quantify Exchange Rates and Affinities of Proteins for Nanoparticles. *Proc. Natl. Acad. Sci. U. S. A.* **2007**, *104*, 2050–2055.

42. Carrstensen, H.; Muller, R. H.; Muller, B. W. Particle Size, Surface Hydrophobicity and Interaction with Serum of Parenteral Fat Emulsions and Model Drug Carriers as Parameters Related to Res Uptake. *Clin. Nutr.* **1992**, *11*, 289–297.
43. Muller, R. H.; Ruhl, D.; Luck, M.; Paulke, B. R. Influence of Fluorescent Labelling of Polystyrene Particles on Phagocytic Uptake, Surface Hydrophobicity, and Plasma Protein Adsorption. *Pharm. Res.* **1997**, *14*, 18–24.
44. Norman, M. E.; Williams, P.; Illum, L. Human Serum Albumin as a Probe for Surface Conditioning (Opsonization) of Block Copolymer-Coated Microspheres. *Biomaterials* **1992**, *13*, 841–849.
45. Sahay, G.; Alakhova, D. Y.; Kabanov, A. V. Endocytosis of Nanomedicines. *J. Controlled Release* **2010**, *145*, 182–195.
46. Renard, C.; Vanderhaeghe, H. J.; Claes, P. J.; Zenebergh, A.; Tulkens, P. M. Influence of Conversion of Penicillin G into a Basic Derivative on Its Accumulation and Subcellular Localization in Cultured Macrophages. *Antimicrob. Agents Chemother.* **1987**, *31*, 410–416.
47. Tulkens, P. M. Intracellular Distribution and Activity of Antibiotics. *Eur. J. Clin. Microbiol. Infect. Dis.* **1991**, *10*, 100–106.
48. Andersen, O. S. Elementary Aspects of Acid-Base Permeation and pH Regulation. *Ann. N.Y. Acad. Sci.* **1989**, *574*, 333–353.
49. Vaudaux, P.; Waldvogel, F. A. Gentamicin Antibacterial Activity in the Presence of Human Polymorphonuclear Leukocytes. *Antimicrob. Agents Chemother.* **1979**, *16*, 743–749.
50. Trouillet, S.; Rasigade, J. P.; Lhoste, Y.; Ferry, T.; Vandenesch, F.; Etienne, J.; Laurent, F. A Novel Flow Cytometry-Based Assay for the Quantification of *Staphylococcus Aureus* Adhesion to and Invasion of Eukaryotic Cells. *J. Microbiol. Methods* **2011**, *86*, 145–149.
51. Toyooka, K.; Takai, S.; Kirikae, T. *Rhodococcus Equi* Can Survive a Phagolysosomal Environment in Macrophages by Suppressing Acidification of the Phagolysosome. *J. Med. Microbiol.* **2005**, *54*, 1007–1015.